Cement and Concrete Research 42 (2012) 889–902

Contents lists available at SciVerse ScienceDirect

Cement and Concrete Research

journal homepage: http://ees.elsevier.com/CEMCON/default.asp

Bayesian calibration of thermodynamic parameters for geochemical speciation modeling of cementitious materials

S. Sarkar [a], D.S. Kosson [a,*], S. Mahadevan [a], J.C.L. Meeussen [b], H. van der Sloot [c], J.R. Arnold [a], K.G. Brown [a]

[a] Department of Civil and Environmental Engineering, Box 1831-B, Vanderbilt University, Nashville, TN 37235, United States
[b] Nuclear Research and Consultancy Group, PO Box 25, NL-1755 ZG Petten, The Netherlands
[c] Hans van der Sloot Consultancy, Dropsstraat 216, 1721 BV Langedijk, The Netherlands

ARTICLE INFO

Article history:
Received 12 October 2011
Accepted 9 February 2012

Keywords:
Bayesian calibration
Thermodynamic parameters
Cement (D)
Geochemical speciation

ABSTRACT

Chemical equilibrium modeling of cementitious materials requires aqueous–solid equilibrium constants of the controlling mineral phases (K_{sp}) and the available concentrations of primary components. Inherent randomness of the input and model parameters, experimental measurement error, the assumptions and approximations required for numerical simulation, and inadequate knowledge of the chemical process contribute to uncertainty in model prediction. A numerical simulation framework is developed in this paper to assess uncertainty in K_{sp} values used in geochemical speciation models. A Bayesian statistical method is used in combination with an efficient, adaptive Metropolis sampling technique to develop probability density functions for K_{sp} values. One set of leaching experimental observations is used for calibration and another set is used for comparison to evaluate the applicability of the approach. The estimated probability distributions of K_{sp} values can be used in Monte Carlo simulation to assess uncertainty in the behavior of aqueous–solid partitioning of constituents in cement-based materials.

1. Introduction and objectives

Cementitious materials exposed to aggressive environmental conditions (e.g., sulfate and chloride attack, carbonation, leaching, aging) degrade over time which eventually leads to performance degradation and potential failure of the structure or its intended characteristics (e.g., as a hydraulic or contaminant release barrier). One of the most important components in numerical modeling of the degradation of cementitious materials under chemical attack is accurate simulation of the chemical reactions between ingressing species and cement hydration products. Challenging issues in this regard include — (1) determining the cement hydration products present in a hardened, matured structure before exposure to the environment, and (2) selecting chemical reactions that may take place when the structure is exposed to aggressive species. Determination of cement hydration products initially present in a matured material can be performed experimentally [1,2] or using cement hydration models [3–6]. Most numerical models only select a limited set of chemical reactions [7–9], and a limited set of available numerical models include flexible platforms that incorporate thermodynamic information for simulating chemical reactions [10,11]. None of these models accounts for the uncertainty that may be present due to the various assumptions and approximations in the model (model uncertainty), variability in the physical parameters or errors in experimental measurements.

A considerable amount of research has been reported on the forward propagation of assumed uncertainty in the chemical equilibrium models in geochemistry and geophysics [12,13]; but the inverse problem of uncertainty quantification in the chemical equilibrium modeling has not received much attention. Two key uncertainties in many currently available geochemical speciation and reactive transport models are the phases selected to represent the chemical system and the assumption of local equilibrium for estimating the equilibrium phases. A majority of these models treat the thermodynamic data obtained from the literature deterministically. However, the K_{sp} values are always determined indirectly and these values do not consider the inherent randomness of the physical parameters, uncertainty in the laboratory conditions under which these values were determined or human error. The uncertainty in chemical equilibrium constants can also be observed in various thermodynamic databases [14–16]. In addition, the mineral phases are most likely present as assemblages with impurities rather than pure phases, which may impact the equilibrium constants. This introduces more uncertainty in the aqueous–solid partitioning behavior. The inadequate description of the chemical state of the materials further adds to the overall uncertainty. Thus treating equilibrium constants deterministically may not allow broader understanding of the domain of expected system behavior. In this paper, the initial K_{sp} values are obtained from the

* Corresponding author.
E-mail addresses: sohini.sarkar@vanderbilt.edu (S. Sarkar), david.kosson@vanderbilt.edu (D.S. Kosson), sankaran.mahadevan@vanderbilt.edu (S. Mahadevan), meeussen@nrg.eu (J.C.L. Meeussen), hans@vanderslootconsultancy.nl (H. der Sloot), joshua.r.arnold@vanderbilt.edu (J.R. Arnold), kevin.g.brown@vanderbilt.edu (K.G. Brown).

0008-8846/$ – see front matter © 2012 Elsevier Ltd. All rights reserved.
doi:10.1016/j.cemconres.2012.02.004

literature and then they are calibrated to reflect the uncertainty arising from various sources such as (i) the assumptions and approximations in the model, i.e., the model uncertainty, (ii) physical variability due to inherent randomness of the material and boundary conditions, and (iii) measurement error. In this respect, it is important to mention that the model chosen affects the calibration. Thus the results obtained are dependent on the model features such as primary ions chosen and mineral set chosen. Quantifying the overall uncertainty in the K_{sp} values arising from the above-mentioned three sources can help more fully explicate the uncertainty in predictions of potential system performance.

A numerical framework is developed in this paper for calibrating the equilibrium constants of a geochemical speciation model for cementitious materials under uncertainty. The uncertainty quantification is performed using a Bayesian statistical method in conjunction with adaptive Markov Chain Monte Carlo (MCMC) simulation techniques. First, the experimental data used for calibration of K_{sp} values and evaluation of applicability of the method are described. Then the geochemical speciation model used for estimating liquid–solid equilibrium is described. Next, the Bayesian statistical approach is used to calibrate the geochemical speciation model using one set of experimental data on the leaching behavior of cementitious materials. Finally, the application of the resulting probability distributions for K_{sp} values is compared with another set of experimental observations from a material with a different mix design.

2. Materials and aqueous–solid partitioning data

Two types of cementitious materials were selected for evaluation in this paper

(i) cements mixed with slag (samples A1 and A2), and
(ii) cements mixed with slag and fly ash (samples B1, B2 and B3).

Notably, samples A1, B1 and B2 were of U.S. origin and testing (Vanderbilt University, Nashville, TN) while samples A2 and B3 were of EU origin and testing (Energy Research Centre of The Netherlands, Petten, NL). Each of these materials was evaluated for equilibrium aqueous–solid partitioning of constituents using standard leaching tests.

2.1. Cements with slag

The two samples evaluated that were formulated with Portland cement and blast furnace slag were

(i) sample A1, composed of Type I/II cement mixed with 40% (by mass) ground granulated blast furnace slag with 1:1.6:2.6 (by mass) binder to sand to gravel ratio and water-binder ratio of 0.38 (by mass), and
(ii) sample A2, prepared from CEM III/B 32.5N cement containing 66% (by mass) ground granulated blast furnace slag with binder to sand ratio 1:3 (by mass) and water-binder ratio 0.5 (by mass).

Table 1
Oxide compositions of the cement samples with slag.

Oxide	Sample A1 60% cement + 40% ground granulated blast furnace slag	Sample A2 34% cement + 66% ground granulated blast furnace slag
SiO_2	28.21	31.00
Al_2O_3	6.98	9.41
Fe_2O_3	2.25	1.28
CaO	52.94	48.53
Na_2O	0.14	0.32
K_2O	0.33	0.34
MgO	5.59	5.85
SO_3 tot.	2.38	2.70

Table 2
Oxide compositions of the cement-based samples with slag and fly ash.

Oxide	Sample B1 30% cement + 40% ground granulated blast furnace slag + 23% fly ash + 7% silica fume	Sample B2 23% cement + 52% ground granulated blast furnace slag + 25% fly ash	Sample B3 48% cement + 32% ground granulated blast furnace slag + 20% fly ash
SiO_2	40.75	38.57	32.89
Al_2O_3	11.94	13.59	10.89
Fe_2O_3	3.32	3.01	2.90
CaO	33.51	33.49	40.49
Na_2O	0.22	0.25	0.29
K_2O	1.01	0.99	1.03
MgO	6.01	7.01	5.64
SO_3 tot.	1.50	1.63	3.22

The oxide compositions of the samples are given in Table 1. The experimental data consist of the concentrations of 6 components (i.e., Al, Ca, Fe Mg, Si and S) at 9 pH values between 1 and 13.

2.2. Cements with slag and fly ash

The three Portland cement-based samples mixed with slag and fly ash were

(i) sample B1, composed of Type V cement mixed with 40% (by mass) ground granulated blast furnace slag, 23% fly ash and 7% silica fume with binder to sand to gravel ratio 1:1.3:2.7 (by mass) and water-binder ratio 0.38 (by mass),
(ii) sample B2, prepared Type I/II cement containing 52% (by mass) ground granulated blast furnace slag and 25% (by mass) fly ash with binder to sand ratio of 1:2.4 (by mass) and water to binder ratio of 0.38 (by mass), and
(iii) sample B3, prepared from a Type V/A 32.5N cement containing 32% (by mass) of ground granulated blast furnace slag and 20% (by mass) fly ash with binder to sand ratio 1:3 (by mass) and water to binder ratio 0.5 (by mass). The oxide compositions of the specimens are given in Table 2.

Similar to Section 2.1, the experimental data consist of the concentrations of 6 components (i.e., Al, Ca, Fe Mg, Si and S) at 9 pH values between 1 and 13.

2.3. Aqueous–solid partitioning experimental data

Aqueous–solid partitioning of selected components as a function of pH was obtained using either EPA Method 1313 ([17]; for samples A1, B1 and B2) or CEN/TS14429 ([18]; for samples A2 and B3). EPA Method 1313 is an equilibrium-based leaching test designed to provide aqueous extracts representing the liquid–solid partitioning (LSP) curves of constituents as a function of eluate pH. This parallel batch procedure consists of nine extractions at targeted pH values and one extraction at the natural pH[1] of the material at room temperature (21±2 °C) [17]. The solid material is particle-size reduced to facilitate the approach to solid–liquid equilibrium. Dilute nitric acid or base (sodium or potassium hydroxide) in deionized water with a final L/S of 10 mL/g-dry is used to achieve final extract pH values at specified target values ranging between 1 and 13. Eluate concentrations for constituents of interest are plotted as a function of eluate pH allowing for comparison to quality control and assessment limits. Results also provide a pH titration curve for each material. CEN/

[1] The natural pH (also referred to as "own pH") is the final eluate pH response of a deionized water extraction of a solid material (i.e., no acid or base added) conducted at an L/S 10 mL/g-dry.

Table 3
Mineral set chosen for geochemical speciation modeling [5,25].

Mineral Phase	Expanded Formula	Common Name	$\log_{10}K_{sp}$
$C_6A\bar{S}H_{32}$	$6CaO\cdot Al_2O_{3.32H_2O}$	Ettringite	-57.09
C_3AH_6	$3CaO\cdot Al_2O_{3.6H_2O}$	Hydrogarnet	-81.15
C_3FH_6	$3CaO\cdot Fe_2O_{3.6H_2O}$	Fe-Hydrogarnet	-74.03
C_2ASH_8	$2CaO\cdot Al_2O_3\cdot SiO_{2.8H_2O}$	Stratlingite	-50.23
C_2FSH_8	$2CaO\cdot Fe_2O_3\cdot SiO_{2.8H_2O}$	Fe-Stratlingite	-43.43
$C_{1.67}SH_{2.1}$	$1.67CaO\cdot SiO_{2.21H_2O}$	Jennite	-29.42
CH	$CaO\cdot H_2O$	Portlandite	-22.80
$C\bar{S}H_2$	$CaO\cdot SO_{3.2H_2O}$	Gypsum	4.60
$Al(OH)_3$ (amorphous)	-	Gibbsite	-9.24
$C_2S_{2.4}H_{3.2}$	$2CaO\cdot 2.4SiO_{2.32H_2O}$	Tobermorite-I	-28.03
$C_{0.83}SH_{1.3}$	$0.83CaO\cdot SiO_{2.13H_2O}$	Tobermorite-II	-11.26
SiO_2	-	Silica	2.71
$Fe(OH)_3$	-	Ferric Hydroxide	-5.00
$C_6F\bar{S}H_{32}$	$6CaO\cdot Fe_2O_{3.32H_2O}$	Fe-Ettringite	-55.19
$Mg(OH)_2$	-	Brucite	-16.84
$CaO\cdot CO_2$	-	Calcite	-7.20
M_4ACH_9	$4MgO\cdot Al_2O_3\cdot CO_{2.8H_2O}$	CO_3-Hydrotalcite	-67.53

TS14429 is very similar to EPA Method 1313. The main difference is that the end pH values in CEN/TS14429 are not as fixed as those in EPA Method 1313. It is stated in the CEN/TS14429 that the deviation between pH at times 44 and 48 h from the start of the experiment shall not exceed 0.3 pH units. Acid or base addition between cumulative extraction times of 44 and 48 h shall not exceed 2% of maximum. An inter-laboratory validation study has shown that both methods provide results that cannot be distinguished within method uncertainty [19]. Results for a wide range of materials, test conditions and constituents have been compiled in a LeachXS database [20–23] and the test results for the samples used in this study were drawn from the LeachXS compilation.

3. Geochemical speciation model for aqueous–solid equilibrium

The geochemical speciation code, ORCHESTRA [24], was used to numerically model the leaching behavior of the materials evaluated in this paper. The chemical reaction equations were written in terms of the selected primary species Al^{+3},Ca^{+2},Fe^{+3},Mg^{+2}, H_4SiO_4,SO_4^{-2},H_2CO_3 and H^+. The simulations were performed by including all aqueous complexes available for these components in the MINTEQ database [25], as well as the mineral phases chosen from Cemdata2007 [5] and MINTEQ database [25] as listed in Table 3. The activity coefficients were calculated using Davies' equation [26] at room temperature (25 °C) assuming a constant ionic strength of 0.1 mol/L. A preliminary sensitivity analysis showed that the difference in leaching behavior of the selected components with and without the assumption of constant ionic strength of 0.1 mol/L was insignificant for this simulation. Thus the constant ionic strength was assumed in this paper. All mineral precipitation–dissolution reactions were assumed to be under local equilibrium condition. Reaction kinetics was not taken into account in this work, as information on kinetic rates for most of the minerals are not available in the existing literature. Alternatively, treating the kinetic rates as calibration parameters would require more than the available data. In this paper, K_{sp} values of the mineral phases are used as calibration parameters. On the other hand, K_{sp} values of the minerals as well as the complex ions or only the complex ions could have been chosen to reflect the uncertainty arising from various sources. However,

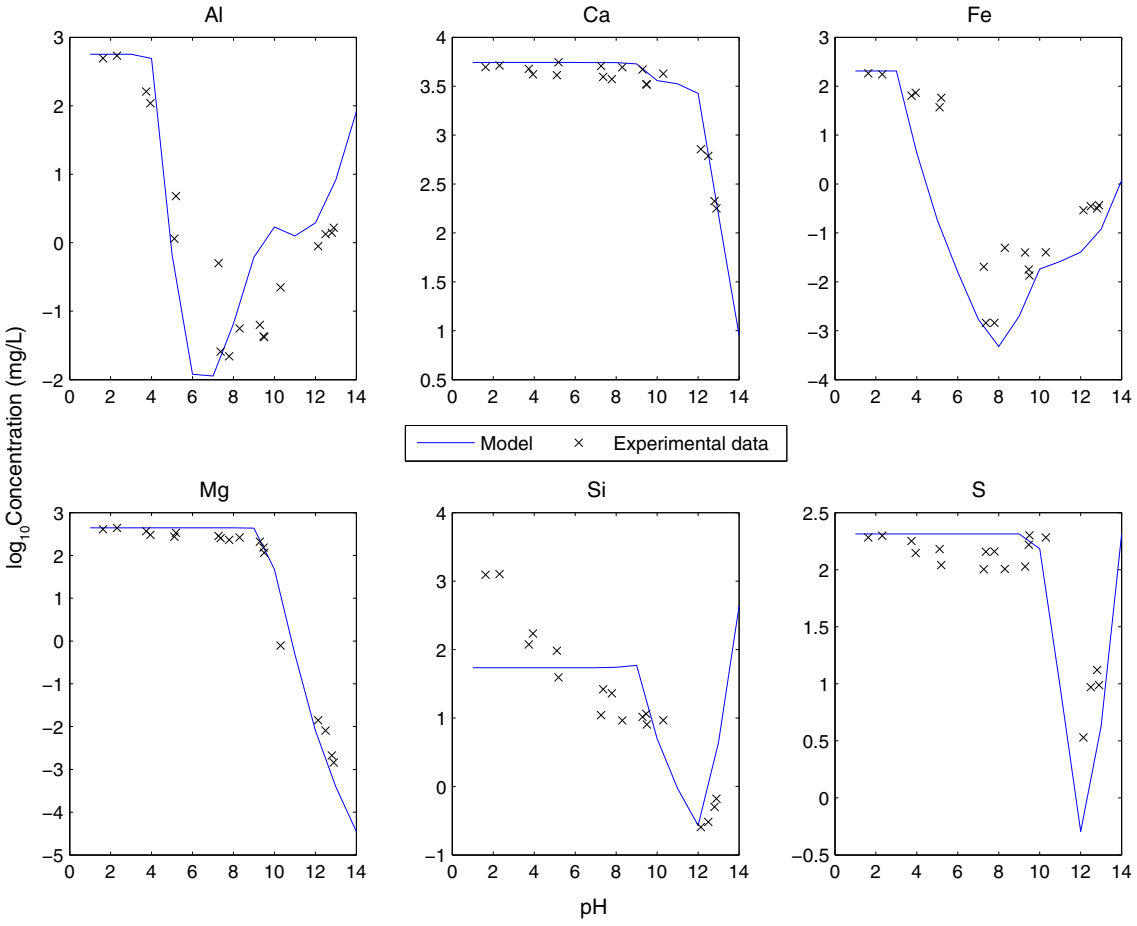

Fig. 1. Comparison of model predictions of total dissolved concentrations of six components with experimental results for sample A1.

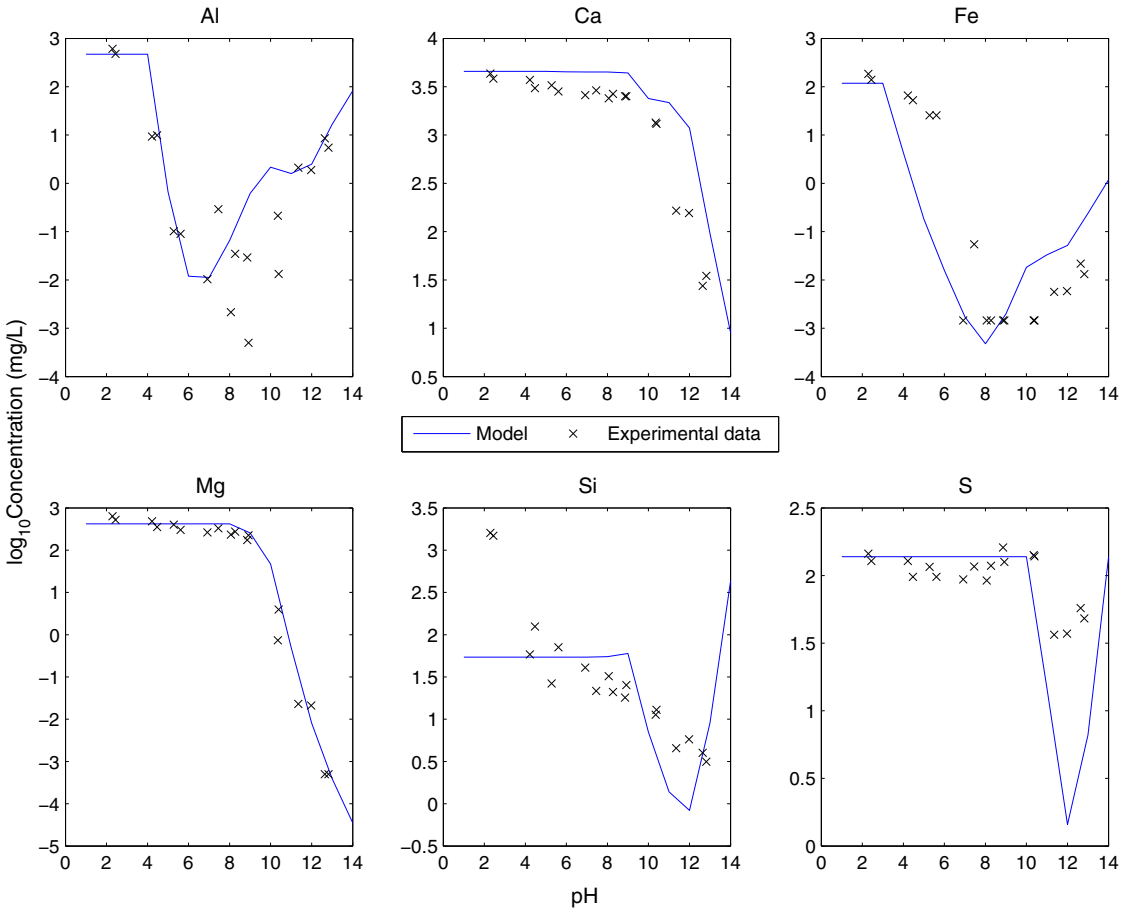

Fig. 2. Comparison of model predictions of total dissolved concentrations of six components with experimental results for sample B1.

calibrating all the K_{sp} values of the minerals as well as the complex ions requires more data than was available. Therefore, only the mineral phases were chosen to reflect uncertainty. The general calibration framework as explained in this paper, would be equally applicable in any of the aforementioned cases (only minerals, only complex ions, both minerals and complex ions).

Initially, the mineral set (i.e., a set of precipitation–dissolution reactions) must be selected that represents the chemical composition of the material, partitioning of chemical species between the pore solution and solid phases, and the minerals that may form as a result of chemical reactions. The mineral set was represented as a set of possible reactions and equilibrium constants (K_{sp} values) as obtained from literature. The inputs to the ORCHESTRA geochemical speciation model are the initial available concentrations of the components and the pH of the solution in which the samples are immersed. The initial available concentrations of the components were obtained by selecting the maximum leached amounts of the components within the pH range of 1 to 13. These values were assumed to be the maximum amounts available for chemical reaction and less than or equal to the total amounts present in the system. The model calculates the liquid–solid equilibrium phases given the set of minerals present in the system and calculates the total dissolved amounts of the components at different pH conditions.

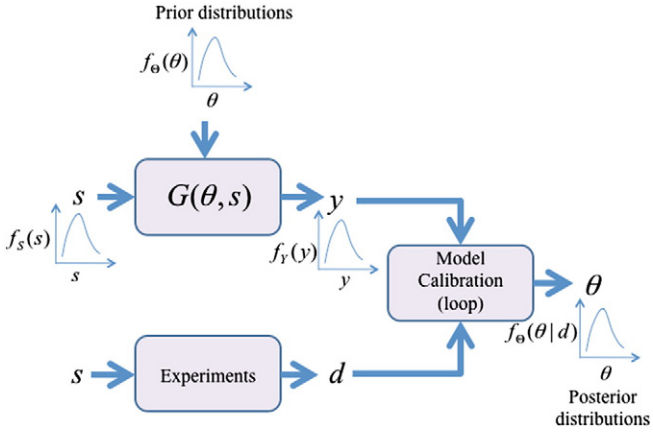

Fig. 3. General framework for model calibration under uncertainty using experimental observations.

A set of 17 minerals was chosen (Table 3) as the final set based on literature reports [5,25] and by comparing the simulation results with the experimental observations of samples A1 and B1 (Tables 1 and 2 in Section 2), after several preliminary trial runs with different mineral sets. Among these minerals, calcium silicate hydrate was modeled using four phases, as a combination of two concurrent solid solution system [5,27] — (i) mixture of amorphous silicon dioxide and Tobermorite-I and (ii) mixture of Jennite and Tobermorite-II. The rest of the minerals were treated as pure phases. The model predictions of total dissolved concentrations of six components (i.e., Al, Ca, Fe, Mg, Si and S) using the selected mineral set for the samples A1 and B1 are shown in Figs. 1 and 2. It is important to mention that a good model prediction could not be achieved for Silicon in the low pH region (pH<7) using several combinations of mineral phases including the combinations recommended for cementitious materials in the literature [5,6,11]. A possible explanation would be that at low pH range the Si concentration is not determined by equilibrium but by slow reaction kinetics, which was not included in the current

model set-up. However, the deviation at low pH does not affect the calculations in the alkaline pH range. In municipal solid waste incineration (MSWI), bottom ash clay formation has been observed during aging under exposure to moisture and contact with the atmosphere [28]. Similar processes may lead to formation of more soluble Si-containing phases upon carbonation of cement-based products as well, which could explain the dissolution behavior as well. However, the lowest pH observed in low-pH cements is around pH 9 [29,30] and remains about pH 7 even after carbonation. Therefore, the deviation in the Si model predictions for pH<7 was not addressed in this paper. However, the model reproduced the trends in the behavior of the other components over the whole pH domain. Thus the experimental results for the other components were kept in the simulation for the sake of completeness. It can be observed from Figs. 1 and 2 that the model reproduced the trends in the leaching behavior of the samples. However, the scatter in the data cannot be captured using a deterministic model. The scatter in the data may come from uncertainty in the experimental measurements and material heterogeneity; the differences between experimental results and model predictions are further confounded by uncertainty in various model parameters and assumptions. Quantification of uncertainty in directly measurable parameters, such as concentrations of species and pH, is generally performed by using measured data. Uncertainty in the model parameters (unobservable or not directly measurable) can be quantified by updating the model parameters using Bayesian statistical inference.

4. Bayesian calibration framework

In Fig. 3, $G(\theta, s)$ represents a numerical model in general. The model can be a simple equation, a set of simultaneous equations (such as the chemical equilibrium model, ORCHESTRA, used here), or a multi-scale, multi-physics coupled model. In the figure, θ is an array of model parameters (having one or more values), s is an array of inputs (having one or more values), and y is a scalar array or a matrix of output variables (such as aqueous concentrations as a function of pH as in the problem being addressed in this paper). In many cases, $y = G(\theta, s)$ does not represent an explicit relationship between inputs and outputs (e.g., in the problem being addressed in this paper). In this case, the expression represents a set of aqueous–solid chemical equilibrium equations, containing several assumed unknown coefficients denoted as model parameters (i.e., K_{sp} values). The solution of the speciation calculation provides leached concentrations (y) of one or more species. In the particular case addressed in the paper, the model parameters are the equilibrium constants (θ) and the input parameters (s) are the concentrations of the species initially present in the system at time ($t = 0$). The parameter y is a one dimensional array of the model realizations composed of concentrations of one species at the end of the simulation; it is a multidimensional array if the model realization provides the concentrations of more than one species. If experimental observations (a single value, an array or matrix of values) are available (d), the model can be calibrated to obtain information about the unobservable model parameters, θ.

There are typically three ways of calibrating a model

(1) The least squares method [31,32]: The sum of the squared errors between model prediction and experimental observations is minimized to obtain a single set of model parameters. This method assumes symmetric error distributions and therefore yields symmetric confidence intervals of the fitted parameters, which may not be appropriate if there are asymmetric (non-normally distributed) errors in the underlying chemical model and experimental results.
(2) The maximum likelihood estimation: The probability of observing the model parameters is maximized to obtain a single set of model parameters [31,33]. The drawbacks of this method are the same as those in the standard least squares method.
(3) The Bayesian method: The input parameters and the errors associated with the observations are treated as random variables [34] to obtain distributions of the model parameters instead of a single set. The asymmetric error in the underlying model and experimental observations can also be incorporated in this flexible model calibration approach. In this paper, the Bayesian model calibration approach is adopted to determine probability distributions for the K_{sp} values of the mineral phases assumed to be present in the cementitious material.

The Bayesian calibration method is based on Bayes' theorem [31] expressed as

$$f(\theta|d) = \frac{f(\theta)f(d|\theta)}{\int f(\theta)f(d|\theta)d\theta} \tag{1}$$

where θ and d are the calibration parameters and the experimental observations, respectively, $f(\theta|d)$ is the probability of observing θ given d (also known as posterior distribution of θ), $f(\theta)$ is the prior knowledge of θ that may be extremely poor (also known as prior distribution of θ), and $f(d|\theta)$ is the probability of observing d given θ (also termed as the likelihood function of θ, i.e., $L(\theta)$). The relation between the experimental observations and the model response is expressed as

$$d = G(\theta, s) + \varepsilon \tag{2}$$

where ε is the overall error due to error in experimental observations, physical variability in the parameters, and various assumptions and approximations made during the modeling process, i.e., model uncertainty. For unbiased observations, ε is generally assumed to have a normal distribution with zero mean and a variance σ^2 where the variance could be assumed, given or calibrated [34,35]. It can also be modeled as a Gaussian process [35]. For this case, the likelihood function, $L(\theta)$, is expressed as

$$L(\theta) = f(d|\theta) = \frac{1}{\sqrt{2\pi}\sigma}\exp\left[-\frac{(d-G(\theta,s))^2}{2\sigma^2}\right]. \tag{3}$$

For a multivariate model output, Eq. (2) transforms into

$$d_i = G(\theta, s) + \varepsilon_i \tag{4}$$

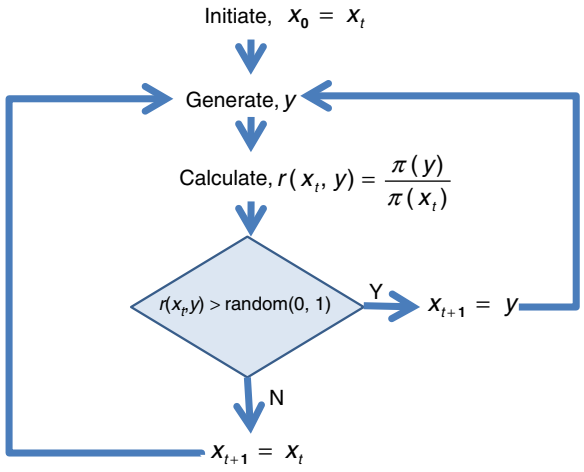

Fig. 4. General framework of Metropolis algorithm for generating samples from an unknown distribution.

where d_i is a multi-element array of observations of ith observable parameter and ε_i is the corresponding error array. The likelihood function is then given by

$$L(\theta) = \prod_{i=1}^{n} f(d_i|\theta) \tag{5}$$

where $f(d_i|\theta)$ is given in Eq. (3). The process of evaluating the posterior distribution, $f(\theta|d)$, becomes challenging if the model is a computer code where no analytical form is available for $f(\theta|d)$. This has been the most significant challenge in implementing the Bayesian method in parameter updating [36]. In such cases, the Markov Chain Monte Carlo sampling method [36,37] has been used to generate the posterior distributions of the parameters.

The denominator on the right hand side of Eq. (1) is a constant and therefore the expression reduces to

$$f(\theta|d) \propto f(\theta) f(d|\theta). \tag{6}$$

If the model parameters are assumed to be independent, the joint prior distribution can be expressed as the product of the prior distributions. Thus Eq. (6) transforms into

$$f(\theta|d) \propto \prod_{j=1}^{m} f(\theta_j) \prod_{i=1}^{n} f(d_i|\theta). \tag{7}$$

4.1. Markov Chain Monte Carlo simulation

The Markov Chain Monte Carlo method is generally used to construct an arbitrary distribution, $\pi(x)$, by drawing samples from the distribution. In this case, x is a specific value of the random variable X. An example of an arbitrary distribution is $f(\theta|d)$ as given in Eq. (6). Here, θ is a specific value of the distribution parameter Θ and d is the observed data. In any time-dependent process, the state of the system at time t is dependent on the previous states up to time $t-1$. This is the basic characteristic of a Markov process where the state of a system at the current iteration step is only dependent on the previous iteration steps. Thus samples drawn from a distribution at a particular iteration step are dependent on the samples drawn at the previous iteration steps. The details of the algorithm used to generate samples from an arbitrary distribution are given next.

There are several algorithms available for generating samples from an unknown distribution using the concept of a Markov process,

Table 4
Model parameter values — prior and posterior medians.

Mineral phase	Prior medians (means) $\log_{10}K_{sp}$	Posterior medians $\log_{10}K_{sp}$	Difference	Skewness
SiO_2	2.71	2.51	0.20	0.18
$C_2S_{2.4}H_{3.2}$	−28.03	−29.24	1.21	−1.22
$C_{1.67}SH_{2.1}$	−29.42	−27.53	−1.89	0.08
$C_{0.83}SH_{1.3}$	−11.26	−12.56	1.30	−0.93
$Mg(OH)_2$	−16.84	−17.07	0.23	−0.08
$CaO \cdot CO_2$	−7.20	−7.31	0.11	−0.14
$Fe(OH)_3$	−5.00	−6.48	1.48	−0.18
$C\bar{S}H_2$	4.60	3.80	0.80	−0.63
CH	−22.80	−22.64	−0.16	−0.58
$C_6A\bar{S}H_{32}$	−57.09	−67.71	10.62	−1.01
$Al(OH)_3$	−9.24	−9.82	0.58	−0.04
C_3AH_6	−81.15	−99.41	18.25	−0.33
C_3FH_6	−74.03	−99.23	25.19	−0.50
$C_6F\bar{S}H_{32}$	−55.19	−53.91	−1.28	−0.90
C_2FSH_8	−43.43	−42.60	−0.82	−0.07
M_4ACH_9	−67.53	−58.81	−8.73	0.30
C_2ASH_8	−50.23	−46.99	−3.23	0.26

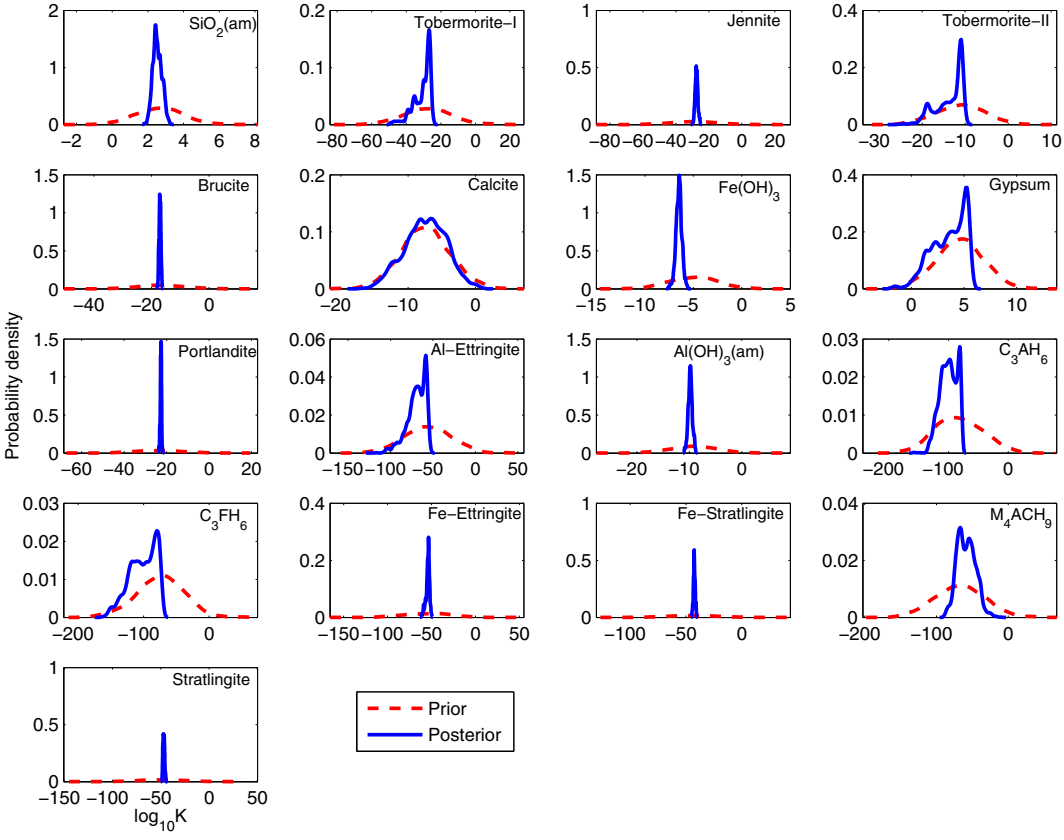

Fig. 5. Prior and posterior distributions of chemical equilibrium constants used in aqueous–solid equilibrium modeling for Sample A1.

e.g., Metropolis algorithm [38], Metropolis–Hastings algorithm [37], Gibbs sampling [39], adaptive Metropolis algorithm [40], delayed rejection method [41]. In this paper, the adaptive Metropolis algorithm combined with the delayed rejection method is used for calibrating the model parameters.

The ultimate goal is to generate samples from the unknown target distribution. As the form of the target distribution is not known, a distribution is proposed which is denoted as the proposal distribution. In the original Metropolis algorithm [38], samples are generated from a symmetric proposal distribution, $q(x)$, such as from assumed uniform, normal, or symmetric triangular distributions. If $q(x)$ is a multivariate distribution, the components of X can be generated sequentially; this process is known as the *single component* Metropolis algorithm. Alternatively, all samples can be generated simultaneously, which is known as the *random walk* Metropolis algorithm [42]. The framework of the Metropolis algorithm, is a special case of the more general Metropolis–Hastings algorithm [37], is shown in Fig. 4.

The algorithm is initialized with a sample, x_t at $t=0$ (i.e., x_0). Then, the next sample, y, is generated from a symmetric proposal distribution, $q(y|x_t)$, centered at the current state. The following expression is evaluated for the candidate sample [41,43]

$$r(x_t, y) = \frac{\pi(y)q(y|x_t)}{\pi(x_t)q(x_t|y)} \tag{8}$$

with the condition that the proposal distribution be symmetric, i.e. $q(y|x_t) = q(x_t|y)$. Therefore, Eq. (8) reduces to $r(x_t,y) = \pi(y)/\pi(x_t)$ as shown in Fig. 4 for the general Metropolis algorithm. Here, $q(x_t|y)$ is the probability of generating x_t from a distribution centered at y and similarly, $q(y|x_t)$ is the probability of generating y from a distribution centered at x_t. The sample, y, is accepted if the ratio, $r(x_t, y) \geq 1$. If $r(x_t, y) < 1$, the sample is accepted with probability $r(x_t, y)$. The method for imposing this condition is to generate a random sample, α, from a uniform distribution between 0 and 1 and if $r(x_t, y) > \alpha$, then the sample is accepted and if $r(x_t, y) < \alpha$, the sample is rejected and then the process is repeated until a sufficient number of samples are generated.

The most common ways of checking the stability and convergence of the algorithm are by evaluating the trace plots of the generated samples and their characteristics. For example, the plots of generated samples and their statistical parameters such as mean and standard deviation, with respect to the number of iterations can be checked for convergence. The distribution constructed from the generated samples is said to have converged to the target distribution if the samples manifest stationary behavior, i.e., statistical evaluation of the samples indicates a constant mean and a constant standard deviation.

The two most important requirements for efficiently executing the algorithm are (i) a good initial value and (ii) a good proposal distribution. The most commonly used proposal distribution for the Metropolis algorithm is a normal distribution with mean at the current sample point and an assumed variance. Rigorous manual tuning is often needed to find an optimum variance [42] for the algorithm to perform efficiently. Several efficient sampling techniques have been proposed to optimize the performance of the algorithm, e.g., adaptive direction sampling [44], the adaptive Metropolis algorithm [42], the adaptive Random Walk method [45], and the delayed rejection method [46]. The adaptive Metropolis algorithm combined with the

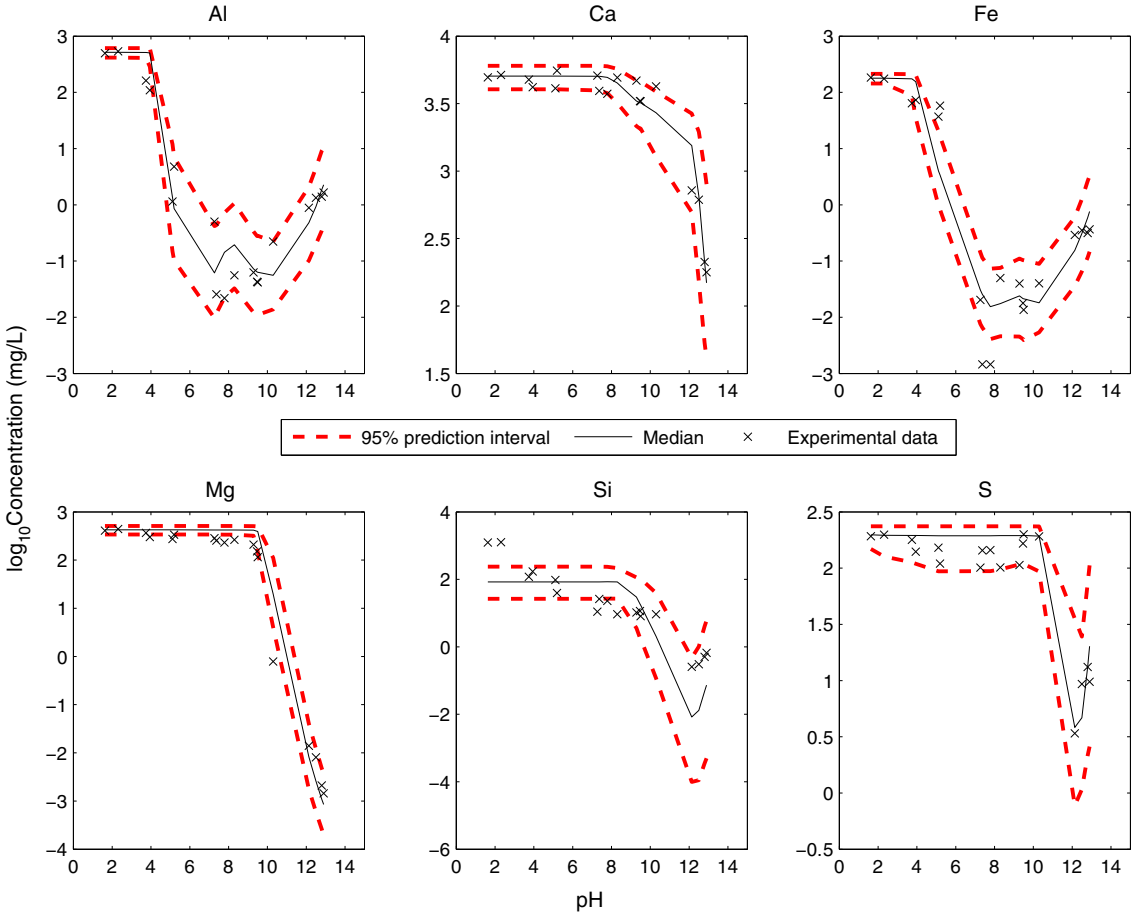

Fig. 6. Median model predictions and 95% prediction intervals of total dissolved concentrations for six components compared to experimental observations of Sample A1. Note: Experimental data at pH<7 for Si were not considered in the calibration.

delayed rejection method [47] is used in this paper to circumvent the problem of manual tuning of the proposal distribution.

4.1.1. Adaptive metropolis algorithm

In the adaptive Metropolis algorithm, the proposal distribution adapts itself automatically using samples generated during the sampling process. Sample generation and acceptance/rejection are first performed as in the original Metropolis algorithm for a certain number of iterations (t_0) assumed by the analyst. Then, the samples are generated from a k-dimensional Gaussian proposal distribution, $N(x_t, C_t)$ with mean x_t and covariance C_t calculated as

$$C_t = \begin{cases} C_0 & t \le t_0 \\ s_d cov(x_0, x_1, \ldots, x_{t-1}) + s_d \epsilon I_k & t > t_0 \end{cases} \quad (9)$$

where C_0 is the initial covariance matrix, s_d is a scaling parameter taken to be $2.4^2/k$ [40,48] because this value has been shown to optimize the performance of Metropolis algorithm for Gaussian targets and Gaussian proposal distributions, ϵ is a very small positive number that prevents the covariance from being zero (in case of rejection of all samples), and I_k is a k-dimensional identity matrix. The covariance matrix is updated after the initial burn-in period ($t_0 = 1000$ iterations in this paper) at an interval of 100 iterations. The steps for calculation of the acceptance ratio and the scheme for determining which of the samples are accepted or rejected are the same as in the original Metropolis algorithm (Fig. 4). This scheme can be applied both in single component and in random walk methods of sample generation. The single component sample generation method takes considerable computational time for high dimensional problems (>15), such as the problem considered in this paper.

The random walk Metropolis algorithm is faster than the single component Metropolis algorithm. A total of N samples (accepted + rejected) are generated in N steps in the random walk scheme, whereas the same number of samples is generated in $N \times k$ steps for the single component scheme, for k dimensional problems. The random walk scheme is more economical than the single component scheme when each simulation realization is computationally intensive. Thus the random walk algorithm is chosen to reduce the number of times the needed chemical equilibrium calculations are performed. But the initial selection of a multivariate proposal distribution is more challenging for the random walk scheme than the single component scheme. The adaptive Metropolis algorithm circumvents the problem of manual selection of the proposal distribution by adapting automatically using generated samples. However, the adaptive Metropolis algorithm is useful only when at least some samples can be generated from the untuned proposal distribution. In this respect, the delayed rejection scheme provides a way of addressing the issue. The adaptive Metropolis method, in conjunction with the delayed rejection scheme (as described in the next section) was selected to enhance the performance of the random walk scheme as well as to gain computational speed.

4.1.2. Delayed rejection method

The basic strategy of the delayed rejection method is that if the newly generated sample from the proposal distribution (termed as first stage proposal distribution) is rejected, instead of staying at the previous sample point, another proposal distribution (termed as

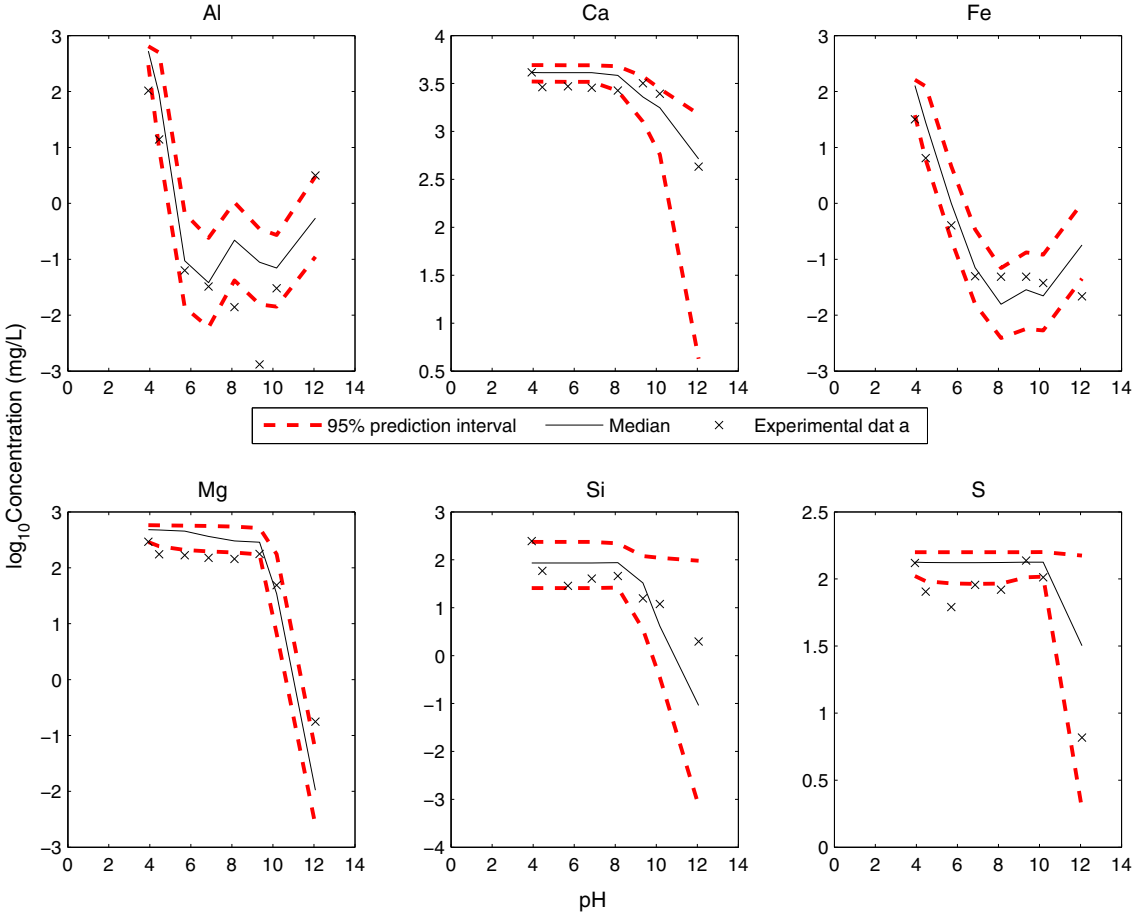

Fig. 7. Median model predictions and 95% prediction intervals of total dissolved concentrations for six components compared to experimental observations of Sample A2. Note: Experimental data at pH<7 for Si were not considered in the calibration.

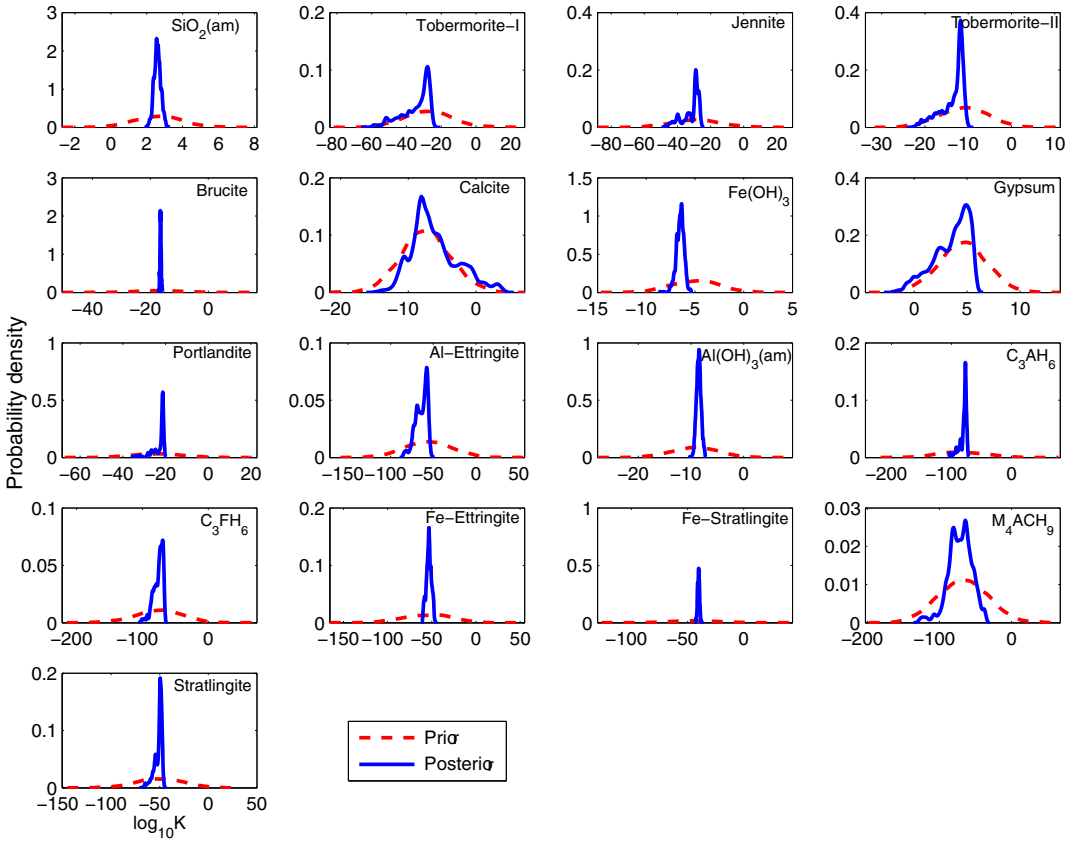

Fig. 8. Prior and posterior distributions of chemical equilibrium constants used in aqueous–solid equilibrium modeling for Sample B1.

second stage proposal distribution) is used to generate the next sample. This process can be repeated as many times as desired. If the process is repeated n times, then the method is commonly known as a n-stage delayed rejection method. Following is a description of a n-stage delayed rejection method.

Let the first stage proposal distribution be $q_1(y_1|x_t)$ that is symmetric and centered at the previous sample x_t. The probability with which the sample is accepted is expressed as

$$r_1(x_t, y_1) = \min\left(1, \frac{\pi(y_1)q_1(y_1|x_t)}{\pi(x_t)q_1(x_t|y_1)}\right) \tag{10}$$

Table 5
Model parameter values — prior and posterior medians.

Mineral phase	Prior medians (means)	Posterior medians	Difference	Skewness
SiO_2	2.71	2.59	0.12	0.02
$C_2S_{2.4}H_{3.2}$	−28.03	−31.73	3.70	−1.03
$C_{1.67}SH_{2.1}$	−29.42	−29.42	0.00	−1.04
$C_{0.83}SH_{1.3}$	−11.26	−12.43	1.17	−1.17
$Mg(OH)_2$	−16.84	−16.47	−0.37	0.15
$CaO\cdot CO_2$	−7.20	−6.81	−0.39	0.62
$Fe(OH)_3$	−5.00	−6.49	1.49	−0.62
$C\bar{S}H_2$	4.60	3.88	0.72	−0.79
CH	−22.80	−21.65	−1.15	−1.80
$C_6A\bar{S}H_{32}$	−57.09	−62.82	5.73	−0.69
$Al(OH)_3$	−9.24	−8.53	−0.72	−0.04
C_3AH_6	−81.15	−77.93	−3.23	−1.59
C_3FH_6	−74.03	−74.15	0.11	−1.05
$C_6F\bar{S}H_{32}$	−55.19	−53.28	−1.91	−0.11
C_2FSH_8	−43.43	−40.22	−3.21	−0.03
M_4ACH_9	−67.53	−70.54	3.00	−0.51
C_2ASH_8	−50.23	−49.91	−0.31	−1.37

which is similar to Eq. (8). If the sample is rejected, another sample, y_2, is generated from a second stage proposal distribution, $q_2(y_2|x_t, y_1)$. The acceptance ratio then is calculated as

$$r_2(x_t, y_1, y_2) = \min\left(1, \frac{\pi(y_2)q_1(y_2|y_1)q_2(y_2|y_1, x_t)[1-r_1(y_2, y_1)]}{\pi(x_t)q_1(x_t|y_1)q_2(x_t|y_1, y_2)[1-r_1(x_t, y_1)]}\right) \tag{11}$$

Similarly, when all the samples from y_1 to y_{n-1} are rejected, the n-th stage acceptance ratio is calculated as

$$r_n(x_t, y_1, y_2, \ldots, y_n) = \min\left(1, \frac{\pi(y_n)q_1(y_n|y_{n-1})q_2(y_n|y_{n-1}, y_{n-2})\ldots q_n(y_n|y_{n-1}, \ldots, x_t)}{\pi(x_t)q_1(x_t|y_1)q_2(x_t|y_1, y_2)\ldots q_n(x_t|y_1, y_2, \ldots, y_n)} \times \frac{[1-r_1(y_n, y_{n-1})][1-r_2(y_n, y_{n-1}, y_{n-2})]\ldots[1-r_{n-1}(y_n, \ldots, y_1]}{[1-r_1(x_t, y_1)][1-r_2(x_t, y_1, y_2)]\ldots[1-r_{n-1}(x_t, y_1, \ldots, y_{n-1})]}\right) \tag{12}$$

The sample, y_n, is accepted if the ratio, $r_n(x_t, y_1, \ldots, y_n) \geq 1$. If $r_n(x_t, y_1, \ldots, y_n) < 1$, the sample is accepted with a probability $r_n(x_t, y_1, \ldots, y_n)$. The analyst may decide to continue with the search of a "good" sample based on the ratio becoming greater than or equal to one. Alternatively, the analyst may decide to limit the number of attempts to a certain value depending on the time requirement of the simulations. In this paper, only two attempts were made to find a "good" sample. If the "good" sample was not found at the end of second attempt, the starting sample was kept at that iteration step. Following Haario et al. [47], the first stage proposal distribution was assumed to be a multivariate normal distribution $N(x_t, C_t)$ where C_t was the covariance matrix as defined in Eq. (9), and the proposal distribution in the following stages was assumed to be a multivariate normal distribution

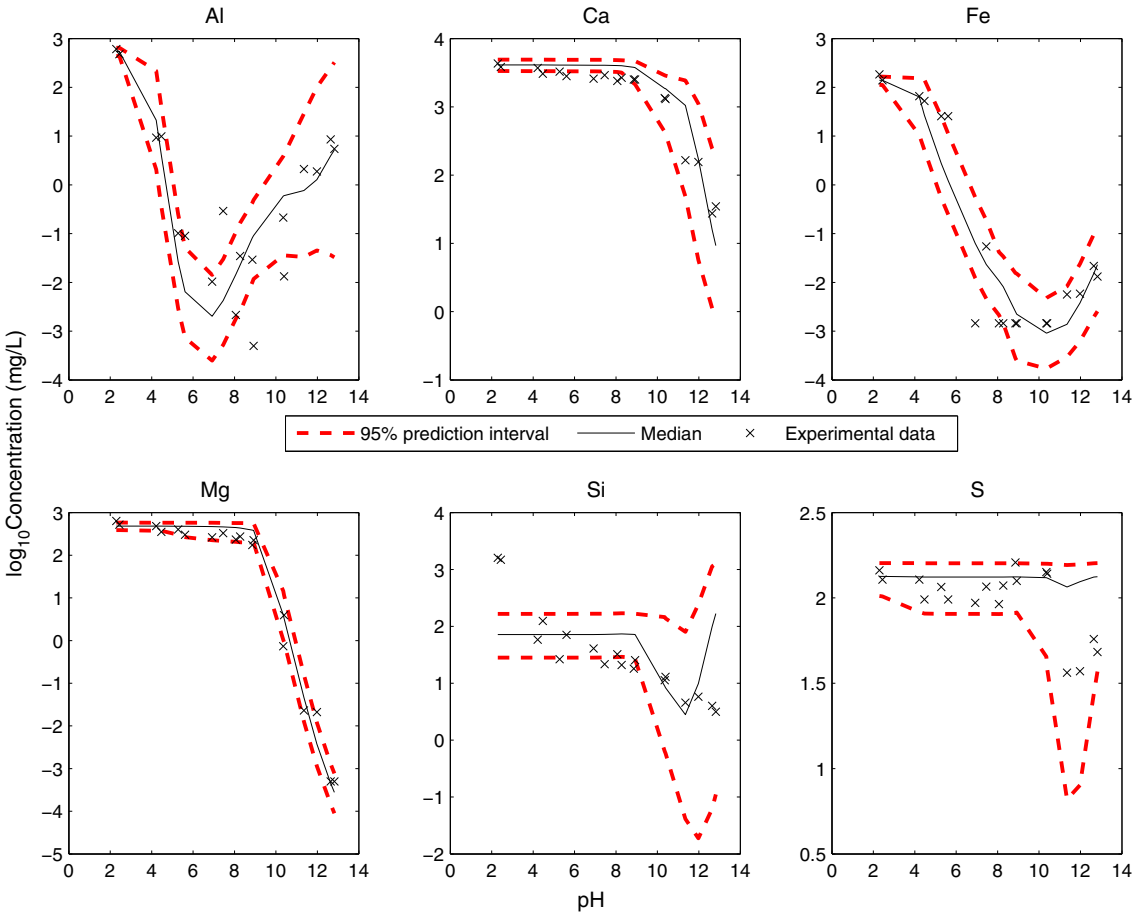

Fig. 9. Median model predictions and 95% prediction intervals of total dissolved concentrations for six components compared to experimental observations of Sample B1. Note: Experimental data at pH<7 for Si were not considered in the calibration.

$N(x_t, C_t^{'})$ where $C_t^{'} = \gamma C_t$ and γ is any positive number less than 1. Haario et al. [47] assumed γ to be 0.01 for a two stage delayed rejection adaptive Metropolis method.

5. Results and discussions

One set of materials was used for calibration of the chemical equilibrium constants and then another set of materials, using the same model and probability distributions for K_{sp} values as determined from the calibration cases, was used as comparison cases to assess the robustness of the approach. The MATLAB implementation of the adaptive Metropolis and delayed rejection adaptive Metropolis schemes (DRAM) by Laine [49] was used in this paper in conjunction with the geochemical speciation code ORCHESTRA for numerically simulating the liquid–solid equilibrium for the cementitious materials. It is important to mention here that even though it was assumed that the model parameters were all independent at the beginning of the simulations, the interdependency of the parameters are reflected in the posterior distributions. Sets of equilibrium constants were generated simultaneously during the Markov Chain Monte Carlo simulation and used in the chemical equilibrium calculations. The interactions of the parameters are reflected through the solutions of the set of simultaneous equations in the chemical equilibrium modeling. Thus the posterior distributions generated using the Markov Chain Monte Carlo approach inherently incorporated dependencies among the model parameters.

The input parameters of the model were the predetermined pH values and the total leachable concentrations of the species obtained from the LeachXS database. The outputs of the model were the total dissolved concentrations of six components (i.e., Al, Ca, Fe, Mg, Si and S) as a function of pH. The difference between the experimental results and model predictions were calculated on log-transformed values as the concentration values vary orders of magnitude and log-transformation allows equal emphasis to be placed on the whole domain of the responses. The following subsections provide the calibration and comparison results for the two cases — (1) cements mixed with slag and (2) cements mixed with slag and fly ash.

5.1. Cements with slag

Sample A1 was chosen for calibration of the model parameters using the Bayesian statistical method. It was assumed that the total leachable concentrations are normally distributed with mean values as obtained from the literature and a 10% coefficient of variation (COV). pH was also assumed to have a normal distribution having mean values at the measured values and 0.1 standard deviation. The prior distributions of the log of the model parameters were assumed to be independent and normally distributed with mean values obtained from the literature and 50% coefficient of variation. A large coefficient of variation was chosen so that the assumed initial prior distribution was not completely non-informative, covered a large range of values, and put more emphasis on the K_{sp} values obtained from the literature. As mentioned previously, the plot of accepted samples vs. iterations show convergence of the generated samples to the target distribution. The posterior (calibrated) distributions were created by using the last 30,000 samples generated after convergence. The calibrated distributions constructed from the generated samples (histograms) were treated as refined distributions.

Alternatively, smooth distributions can be constructed using well-known parametric distributions or nonparametric kernel-density functions. However, the generated samples were directly used in the paper to preserve the correlations among the parameters. Fig. 5 shows the prior (assumed) and posterior (calibrated) distributions of the model parameters. Table 4 shows the medians of prior and posterior distributions (in log-scale), the differences between them, and the skewness of the posterior distributions (a measure of asymmetry of the posterior distributions). It can be observed from Fig. 5 and Table 4 that most of the posterior distributions are much narrower than the prior distributions indicating that very narrow regions of the posterior distributions are supported by the experimental observations. Additionally, none of the posterior distributions except for Calcite retained its original shape. This result suggests low impact of this mineral on the solid–liquid equilibrium of this particular system. Some of the posterior distributions (e.g., Tobermorite-I, Tobermorite-II, Gypsum, and Al-Ettringite) show asymmetry in the figure as well as in the measure of asymmetry (i.e., skewness) in Table 4. This confirms the capability of the Bayesian approach to discover asymmetry, which is not possible with least squares-based calibration. This result also indicates that the mineral-dissolution/precipitation may be kinetically retarded leading to undersaturation of the pore solution with respect to these minerals. 3000 Monte Carlo simulations were then performed by using 3000 sets of equilibrium constants from the posterior distributions of the model parameters. The model predictions were used to calculate 2.5th and 97.5th percentile values to obtain 95% prediction intervals. This method of prediction interval estimation (nonparametric) does not require any assumption regarding the underlying population. Fig. 6 shows the median model predictions and the prediction intervals compared to the experimental results. It can be observed from the figure that the median model predictions capture the trends in the experimental results and the 95% prediction intervals encompass much of the scatter in experimental values.

As cement chemistry is primarily governed by the ratio of the availabilities of various species, the second sample (Sample A2), similar in composition to Sample A1 (Table 1), was used as a comparison case for the calibration results. Fig. 7 shows the 95% prediction intervals, median model predictions and experimental results for Sample A2. As before, it can be observed from the figure that the median model predictions reproduce the trends in the experimental results. The 95% model predictions also encapsulate the majority of the experimental data. Therefore, this approach adequately quantified the uncertainty in the chemical equilibrium modeling and propagated it to represent the uncertainty in the chemical behavior of a similar cementitious material.

5.2. Cements with slag and fly ash

Similar to the previous subsection, Sample B1 was used to calibrate the equilibrium constants. As before, prior distributions of the model parameters were assumed to be Gaussian with mean values obtained from the literature and 50% COV. The available/leachable concentrations of species were assumed to have normal distributions with mean values obtained from the experimental data and 10% COV; pH was assumed to be normally distributed with mean values at the experimental data points and 0.1 standard deviation. Similar to Section 5.1, posterior (calibrated) distributions were created from

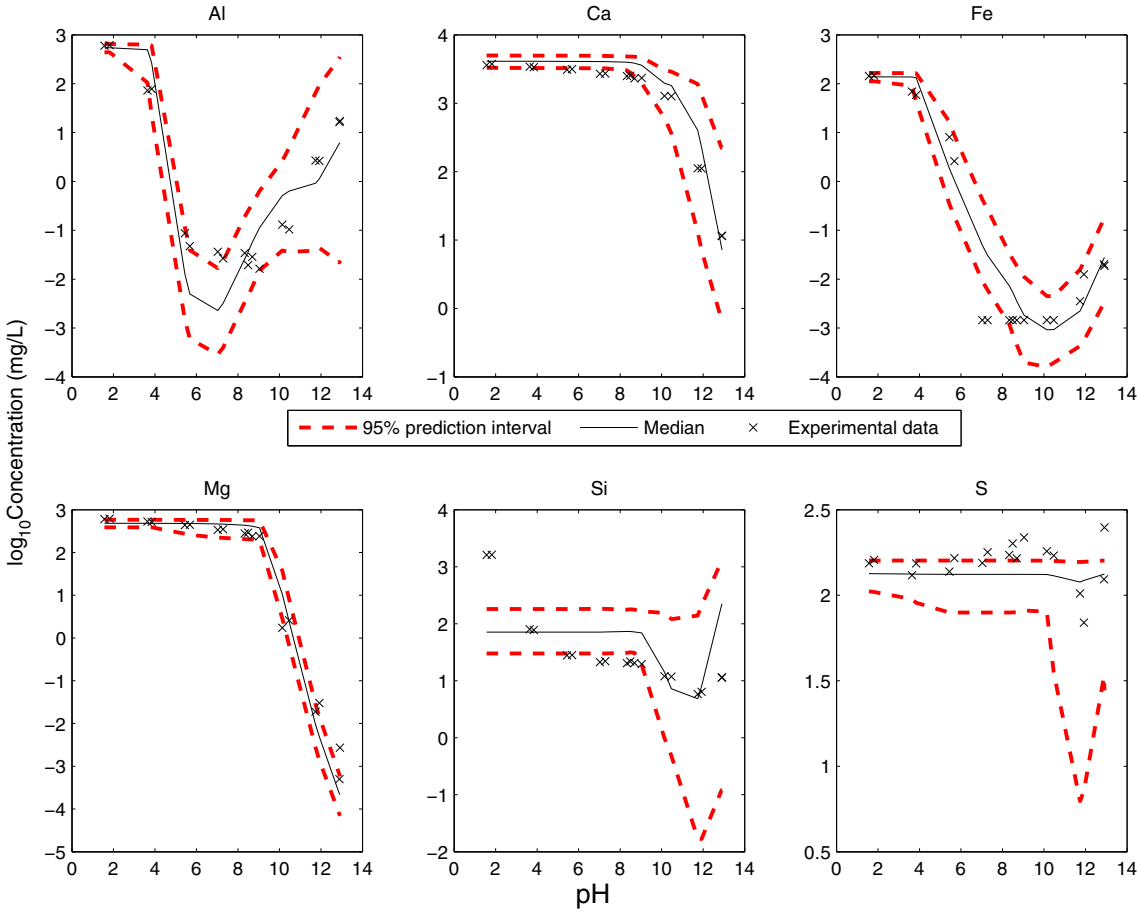

Fig. 10. Median model predictions and 95% prediction intervals of total dissolved concentrations for six components compared to experimental observations of Sample B2. Note: Experimental data at pH<7 for Si were not considered in the calibration.

the last 30,000 samples generated (histograms) after convergence of the generated samples to the target distribution. The generated samples were directly used as the refined distributions to preserve the correlations among the parameters. Fig. 8 shows the prior (assumed) and the posterior (calibrated) distributions. The median values of the equilibrium constants as obtained from the literature, the median values obtained from the posterior distributions, the difference in the median values, and skewness of the posterior distributions are given in Table 5. Similar to the results in Section 5.1, most of the posterior distributions are much narrower than the prior distributions indicating that a very narrow region in the parameter space is supported by the experimental observations. Except Calcite, none of the posterior distributions retained its originally assumed shape. This may be caused by the possibility of low impact of Calcite on the chemical equilibrium simulation. The asymmetry in some of the posterior distributions (e.g., Tobermorite-I, Jennite, Tobermorite-II, Gypsum, and Al-Ettringite) may be caused by kinetic retardation in the formation of the minerals. 3000 Monte Carlo simulations were performed by using 3000 sets of equilibrium constants obtained from the posterior distributions. Fig. 9 shows the 95% prediction intervals estimated from the 2.5th and 97.5th percentile values of the model predictions, median model predictions and the experimental data for Sample B1. The figure shows that the model prediction captures the trends in the experimental data and the prediction interval captures most of the observed data as should be the case for a robust calibration method.

Finally, Samples B2 and B3 (similar in composition to Sample B1) from Table 2 were used as comparison cases for the calibrated distributions of the equilibrium constants. Figs. 10 and 11 show the 95% prediction intervals, median model predictions, and the experimental data for the samples. It is evident from the figures that the model predictions reproduce the trends in the experimental results and the prediction intervals capture most of the scatter in the data.

The results as shown in Figs. 5 and 8 provide useful information regarding the uncertainty in the equilibrium constants obtained from the literature and used in the assumed chemical model, the effect of measurement errors, and the state of knowledge represented by the chemical equilibrium model. The uncertainty arising from the inherent variability in the physical parameters is irreducible. Model uncertainty due to various assumptions and approximations can only be eliminated by improving the knowledge of cement chemistry including kinetics, which would likely require significant experimental and modeling endeavors. Using the current state of knowledge, the uncertainty in the model parameters as quantified using the Bayes' calibration method, combined with the likely impact of experimental errors and physical variability can provide useful information regarding the uncertainty in the chemical equilibrium model. In addition to physical variability of the parameters, chemical parameters (i.e., equilibrium constants) introduce significant additional uncertainty in the model predictions as shown in the model predictions in this section (Figs. 6, 7, 9–11). This may also include the possibility of having an inadequate set of minerals (contributing to model uncertainty). Therefore, it is important to quantify uncertainty in the chemical equilibrium model and incorporate that in the chemical response assessment of cement-based structures.

6. Conclusions

A Bayesian calibration method was used in this paper to quantify uncertainty in the chemical equilibrium model used for cement-

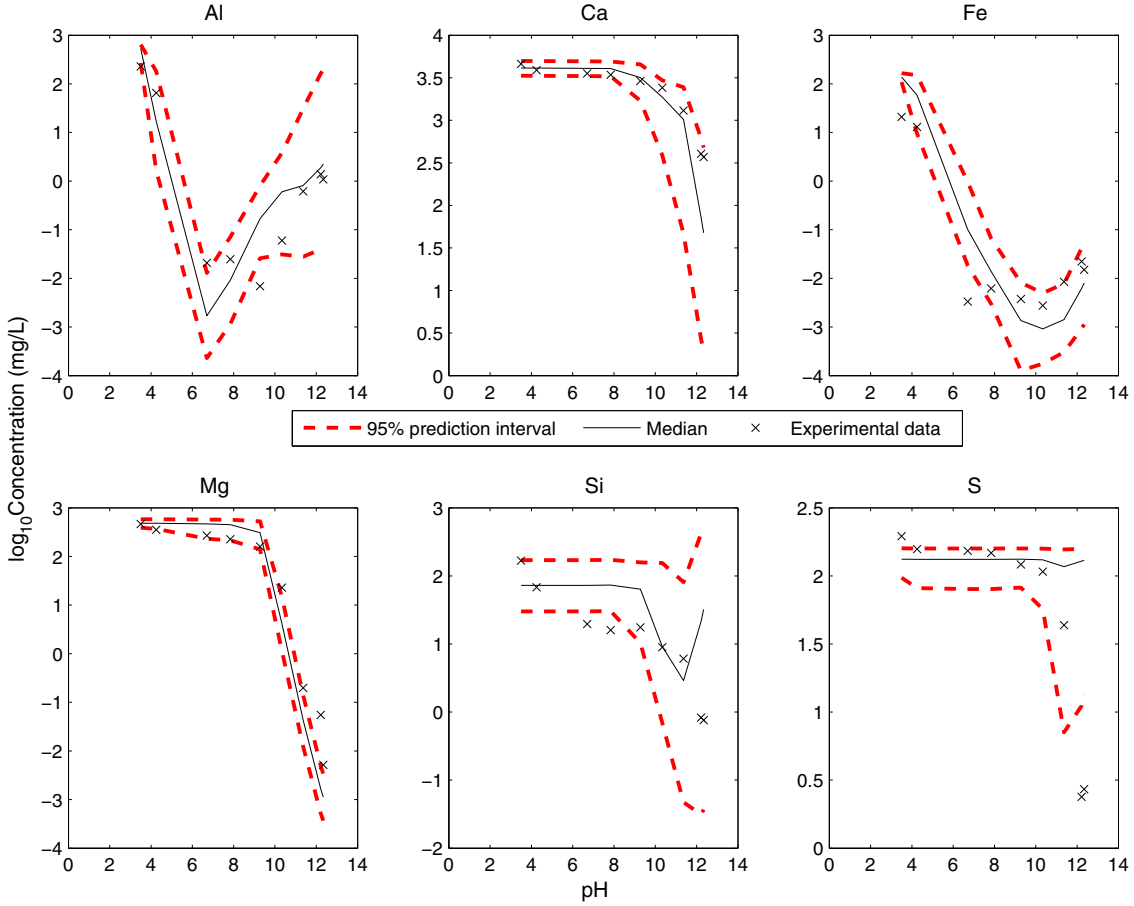

Fig. 11. Median model predictions and 95% prediction intervals of total dissolved concentrations for six components compared to experimental observations of Sample B3. Note: Experimental data at pH<7 for Si were not considered in the calibration.

based materials. A set of 17 mineral phases was chosen to describe the chemical behavior of the materials studied after a preliminary investigation with several mineral sets. First, one set of experimental results on the leaching behavior of cement-based materials was used for calibration of the equilibrium constants, and then another set of experimental data was used for comparison purposes to assess the robustness of the resultant probability distributions for the equilibrium constants. The uncertainty attributed to the chemical equilibrium constants accounts for mainly three sources of uncertainty — (i) physical variability in the material properties and the boundary conditions, (ii) model uncertainty due to various assumptions and approximations in the model, and (iii) measurement error. The key sources of uncertainty in the geochemical speciation of cementitious materials contributing to the model uncertainty are (i) selection of mineral phases, (ii) local equilibrium assumption, (iii) presence of assemblages of mineral phases and probable absence of pure phases, and (iv) uncertainty in the laboratory conditions under which the K_{sp} values were measured. Upon calibration, most of the posterior distributions of the equilibrium constants were observed to be much narrower than the assumed prior distributions, and the asymmetry in some of the posterior distributions may indicate kinetic retardation in the respective mineral precipitation/dissolution. The 95% prediction intervals of the model responses described the scatter in the experimental data, and the median model predictions agreed with the trends in the experimental behavior. Therefore, the uncertainty in the material response as captured by the prediction intervals can be used to assess uncertainty in the chemical behavior of the cementitious materials. The quantified uncertainty in turn, can also be used to inform uncertainty assessment in the prediction of durability of cement-based materials under chemical attacks in a range of applications. However, more cases should be evaluated to assess the applicability of this approach to a wider range of materials and cases.

7. Disclaimer

This report is prepared as an account of work sponsored by an Agency of the United States Government. Neither the United States Government nor any agency thereof, nor any of their employees, makes any warranty, express or implied, or assumes any legal liability or responsibility for the accuracy, completeness, or usefulness of any information, apparatus, product, or process disclosed, or represents that its use would not infringe privately owned rights. Reference herein to any specific commercial product, process, or service by trade name, trademark, manufacturer, or otherwise does not necessarily constitute or imply its endorsement, recommendation, or favoring by the United States Government or any agency thereof.

Acknowledgments

This study was based on work supported by the U. S. Department of Energy, under Cooperative Agreement Number DE-FC01-06EW07053 entitled 'The Consortium for Risk Evaluation with Stakeholder Participation III' awarded to Vanderbilt University. This research was also carried out in part as part of the Cementitious Barriers Partnership supported by U.S. DOE Office of Environmental Management. The opinions, findings, conclusions, or recommendations expressed herein are those of the authors and do not necessarily represent the views of the Department of Energy or Vanderbilt University. The authors also thank Dr. Christine Langton and Dr. Greg Flach (Savannah River National Laboratory), Dr. Eric Samson (SIMCO Technologies), and Dr. Edward Garboczi (National Institute of Standards and Technology) for valuable discussions during this study.

References

[1] D. Planel, J. Sercombe, P. Le Bescop, F. Adenot, J.M. Torrenti, Long-term performance of cement paste during combined calcium leaching-sulfate attack: kinetics and size effect, Cem. Concr. Res. 36 (2006) 137–143.
[2] K.L. Scrivener, Backscattered electron imaging of cementitious microstructures: understanding and quantification, Cem. Concr. Compos. 26 (2004) 935–945.
[3] D.P. Bentz, A three-dimensional cement hydration and microstructure development modeling package. Version 3.0, National Institute of standards and Technology, 2005.
[4] O. Bernard, F.-J. Ulm, E. Lemarchand, A multiscale micromechanics-hydration model for the early-age elastic properties of cement-based materials, Cem. Concr. Res. 33 (2003) 1293–1309.
[5] B. Lothenbach, T. Matschei, G. Möschner, F.P. Glasser, Thermodynamic modelling of the effect of temperature on the hydration and porosity of Portland cement, Cem. Concr. Res. 38 (2008) 1–18.
[6] B. Lothenbach, F. Winnefeld, Thermodynamic modelling of the hydration of Portland cement, Cem. Concr. Res. 36 (2006) 209–226.
[7] B. Bary, Simplified coupled chemo-mechanical modeling of cement pastes behavior subjected to combined leaching and external sulfate attack, Int. J. Numer. Anal. Methods Geomech. 32 (2008) 1791–1816.
[8] M. Basista, W. Weglewski, Chemically assisted damage of concrete: a model of expansion under sulfate attack, Int. J. Damage Mech. 18 (2) (2008) 155–175.
[9] R. Tixier, B. Mobasher, Modeling of damage in cement-based materials subjected to external sulfate attack. I: formulation, J. Mater. Civ. Eng. 15 (2003) 305–313.
[10] C.J. Haecker, E.J. Garboczi, J.W. Bullard, R.B. Bohn, Z. Sun, S.P. Shah, et al., Modeling the linear elastic properties of Portland cement paste, Cem. Concr. Res. 35 (2005) 1948–1960.
[11] E. Samson, J. Marchand, Modeling the transport of ions in unsaturated cement-based materials, Comput. Struct. 85 (2007) 1740–1756.
[12] S.E. Cabaniss, Propagation of uncertainty in aqueous equilibrium calculations: non-Gaussian output distributions, Anal. Chem. 69 (1997) 3658–3664.
[13] K. Schulz, B. Huwe, S. Peiffer, Parameter uncertainty in chemical equilibrium calculations using fuzzy set theory, J. Hydrol. 217 (1999) 119–134.
[14] J.R. Duffield, F. Marsicano, D.R. Williams, Chemical speciation modelling and thermodynamic database compilation—I. Data uncertainties, Polyhedron 10 (1991) 1105–1111.
[15] T. Matschei, Thermodynamics of Cement Hydration, University of Aberdeen, 2007.
[16] O. Nitzsche, G. Meinrath, B. Merkel, Database uncertainty as a limiting factor in reactive transport prognosis, J. Contam. Hydrol. 44 (2000) 223–237.
[17] A.C. Garrabrants, D.S. Kosson, H. Van der Sloo, F. Sanchez, O. Hjelmar, Background Information for the Leaching Environmental Assessment Framework (LEAF) Test Methods (EPA/600/R-10/170), EPA, 2010.
[18] CEN, Characterization of Waste – Leaching Behavior Tests – Influence of pH on Leaching with Initial Acid/Base Addition, CEN, Brussels, Belgium, 2005.
[19] Inter-Laboratory Validation of LEAF Parallel Batch Leaching Tests: Method 1313 and Method 1316, 2011.
[20] H.A. van der Sloot, P. Seignette, R.N.J. Comans, A. van Zomeren, J.J. Dijkstra, H. Meeussen, et al., Evaluation of Environmental Aspects of Alternative Materials using an Integrated Approach Assisted by a Database/Expert System, 2003.
[21] H. van der Sloot, D. Hoede, R.P.J.J. Rietra, R. Stenger, T. Lang, M. Schneider, et al., Environmental Criteria for Cement-Based Products, ECRICEM I, ECN C-01-069, Netherlands Energy Research Foundation, Petten, The Netherlands, 2001.
[22] H. van der Sloot, A. van Zomeren, R. Stenger, M. Schneider, G. Spanka, E. Stoltenberg-Hansson, et al., Environmental CRIteria for CEMent-based products (ECRICEM) phase I: ordinary Portland cements and Phase II: blended cements, executive summary, ECV-E-11-020, Netherlands Energy Research Foundation, Petten, The Netherlands, 2008.
[23] H. van der Sloot, Comparison of the characteristic leaching behaviour of cements using standard (EN 196-1) cement-mortar and an assessment of their long-term environmental behaviour in construction products during service life and recycling, Cem. Concr. Res. 30 (2000) 1079–1096.
[24] J.C.L. Meeussen, ORCHESTRA: an object-oriented framework for implementing chemical equilibrium models, Environ. Sci. Technol. 37 (2003) 1175–1182.
[25] J.D. Allison, D.S. Brown, K.J. Novo-gradac, MINTEQA2, Geochemical Assessment Model for Environmental Systems, Version 3, U.S. Environmental Protection Agency, Washington, DC, 1992.
[26] E. Samson, G. Lemaire, J. Marchand, J.J. Beaudoin, Modeling chemical activity effects in strong ionic solutions, Comput. Mater. Sci. 15 (1999) 285–294.
[27] M.K. Dmitrii, A. Kulik, Aqueous solubility diagrams for cementitious waste stabilization systems: II, end-member stoichiometries of ideal calcium silicate hydrate solid solutions, J. Am. Ceram. Soc. 84 (2001) 3017–3026.
[28] C. Zevenbergen, L.P. van Reeuwijk, J.P. Bradley, P. Bloemen, R.N.J. Comans, Mechanism and conditions of clay formation during natural weathering of MSWI bottom ash, Clays Clay Miner. 44 (1996) 546–552.
[29] D. Sugiyama, T. Fujita, A thermodynamic model of dissolution and precipitation of calcium silicate hydrates, Cem. Concr. Res. 36 (2006) 227–237.
[30] T. Zhang, C.R. Cheeseman, L.J. Vandeperre, Development of low pH cement systems forming magnesium silicate hydrate (M-S-H), Cem. Concr. Res. 41 (2011) 439–442.
[31] A. Haldar, S. Mahadevan, Probability, Reliability, and Statistical Methods in Engineering Design, John Wiley and Sons, 2000.
[32] T.G. Trucano, L.P. Swiler, T. Igusa, W.L. Oberkampf, M. Pilch, Calibration, validation, and sensitivity analysis: what's what, Reliab. Eng. Syst. Saf. 91 (2006) 1331–1357.

[33] K.V. Mardia, R.J. Marshall, Maximum likelihood estimation of models for residual covariance in spatial regression, Biometrika 71 (1984) 135–146.
[34] J. McFarland, S. Mahadevan, V. Romero, L. Swiler, Calibration and uncertainty analysis for computer simulations with multivariate output, AIAA Journal. 46 (2008) 1253–1265.
[35] M.C. Kennedy, A. O'Hagan, Bayesian calibration of computer models, J. R. Stat. Soc. B 63 (2001) 425–464.
[36] B. Walsh, Markov Chain Monte Carlo and Gibbs Sampling, 2002.
[37] W.K. Hastings, Monte Carlo sampling methods using Markov Chains and their applications, Biometrika 57 (1970) 97–109.
[38] N. Metropolis, A.W. Rosenbluth, M.N. Rosenbluth, A.H. Teller, E. Teller, Equation of state calculations by fast computing machines, J. Chem. Phys. 21 (1953) 1087–1092.
[39] S. Geman, D. Geman, Stochastic relaxation, Gibbs distributions, and Bayesian restoration of images, IEEE Trans. Pattern Anal. Mach. Intell. PAMI-6 (1984) 721–741.
[40] H. Haario, E. Saksman, J. Tamminen, An adaptive Metropolis algorithm, Bernoulli 7 (2001) 223–242.
[41] A. Mira, On Metropolis–Hastings algorithms with delayed rejection, Metron LIX (2001) 231–241.
[42] H. Haario, E. Saksman, J. Tamminen, Adaptive proposal distribution for random walk Metropolis algorithm, Comput. Stat. 14 (1999) 375–395.
[43] S. Chib, E. Greenberg, Understanding the Metropolis–Hastings algorithm, Am. Stat. 49 (1995) 327–335.
[44] W.R. Gilks, G.O. Roberts, E.I. George, Adaptive direction sampling, J. R. Stat. Soc. D Stat. 43 (1994) 179–189.
[45] Y.F. Atchade, J.S. Rosenthal, On adaptive Markov chain Monte Carlo algorithms, Bernoulli 11 (2005) 815–828.
[46] L. Tierney, A. Mira, Some adaptive Monte Carlo methods for Bayesian inference, Stat. Med. 18 (1999) 2507–2515.
[47] H. Haario, M. Laine, A. Mira, E. Saksman, DRAM: efficient adaptive MCMC, Stat. Comput. 16 (2006) 339–354.
[48] A. Gelman, G.O. Roberts, W.R. Gilks, Efficient Metropolis jumping rules, Bayesian Statistics 5 (1996) 599–607.
[49] M. Laine, Adaptive MCMC Methods with Applications in Environmental and Geophysical Models, Lappeenranta University of Technology, Mathematics and Physics, 2008.